

# **MODE-MATCHING ANALYSIS OF THE INDUCED ELECTRIC FIELD IN A MATERIAL SAMPLE PLACED WITHIN AN ENERGIZED CYLINDRICAL CAVITY**

J.-P. Zhang and K.-M. Chen

Department of Electrical and Computer Engineering  
Michigan State University  
East Lansing, MI 48824, USA

- 1. Introduction**
- 2. Eigenmodes in an Inhomogeneously Filled Waveguide**
- 3. Electromagnetic Fields in Three Regions**
- 4. Numerical Examples**
  - 4.1 Cubic-Like Material Sample
  - 4.2 Thin Disk Material Sample
  - 4.3 Thin Dielectric Rod Material Sample
- 5. Conclusions**

## **References**

## **1. INTRODUCTION**

In a companion paper [1] published in this issue, an electric field integral equation (EFIE) method was developed to quantify the induced electric field inside a material sample placed in an energized cavity. It was demonstrated that the integral equation method is a powerful technique because it can handle the material sample of arbitrary shapes and heterogeneities. The only disadvantage of this method is its slow numerical convergence and a large computation time. To provide a numerical check for the integral equation method, a mode-matching method is developed in this paper to study the same subject.

We consider a cylindrical cavity coaxially loaded with a homogeneous material sample of simple geometry and excited by a current probe. A mode-matching method combined with a Green's function

technique for the excitation probe is applied to determine the induced electric field inside the material sample as well as the fields in other parts of the cavity. Analytical results of the mode-matching method are then used to verify the numerical accuracy of the integral equation method. It is noted that the mode-matching method can only handle homogeneous material samples with simple geometries. However, it can provide sufficient information for the verification of the integral equation method.

In fact, the mode-matching method has been used by a number of workers to analyze dielectric-loaded cavities [2–6]. These previous studies were mainly concerned with the resonant frequency and the field distribution, and the excitation of a current probe was not considered. Similar problems involving the interaction of the cavity field and a material sample inside a cavity have been studied by other methods, including the surface integral equation method, the finite difference-time domain method, the finite element method and the method of lines [7–13].

Applying the mode-matching method to a homogeneous material sample with a simple cylindrical geometry placed within a cylindrical cavity, we can divide the cavity into three waveguide regions as shown in Fig. 1, where regions I and III are the normal waveguide regions filled with a homogeneous material or empty and region II is the inhomogeneously filled waveguide region containing the material sample. The waveguide eigenmodes in region II are derived first while those in regions I and III are well known. The *EM* fields in each region are expressed in terms of its eigenmodes, and the tangential components of the electric and magnetic fields are matched at the junctions of the three regions. The equations resulted from the matching of the boundary conditions are then numerically solved. The numerical results agree well with that obtained using the integral equation method. It is also shown that the mode-matching method can save a great deal of computation time attributed to the use of the well-defined eigenmodes and sparse resultant matrices.

## 2. EIGENMODES IN AN INHOMOGENEOUSLY FILLED WAVEGUIDE

The geometry of an inhomogeneously filled waveguide is shown in Fig. 2 which consists of two sub-regions having the same central axis. The central sub-region is a homogeneous material sample and the outer

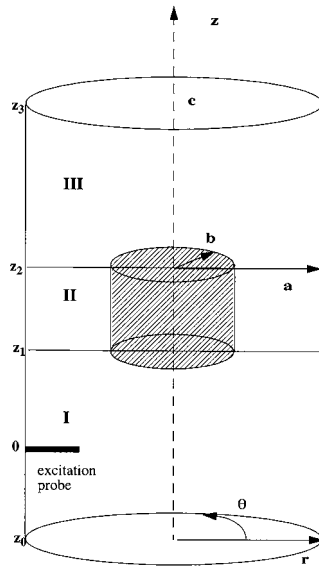


**Figure 1.** Geometry of the material sample placed in a cylindrical cavity driven by an excitation probe.

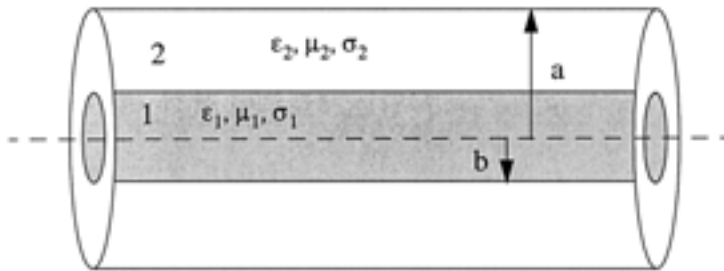


**Figure 2.** Geometry of the inhomogeneously filled waveguide which is region II in Fig. 1.

sub-region is empty space. It is noted that if the material sample has an irregular shape or is heterogeneous, the eigenmodes in such an inhomogeneously filled waveguides will be difficult, if not impossible, to be determined. Therefore, in this paper we only deal with the homogeneous material samples with simple cylindrical geometries which are placed coaxially in the cavity.

The normal eigenmodes in this inhomogeneously filled waveguide are not, in general, either  $TE$  or  $TM$  modes, but a combination of an  $TE$  and an  $TM$  mode, a hybrid eigenmode. An exception is the case of  $n = 0$  modes which will be shown later.

In Fig. 2, the dielectric parameters of sub-region 1 are: relative permittivity  $\varepsilon_1$ , permeability  $\mu_1$  and conductivity  $\sigma_1$ , and its radius  $b$ . The parameters of sub-region 2 are: relative permittivity  $\varepsilon_2$ , permeability  $\mu_2$  and conductivity  $\sigma_2$  with radius  $a$ . Based on the relations between the longitudinal and the transverse components of the electromagnetic fields given in [14], we obtain the electromagnetic eigenmodes in these two sub-regions when  $n \neq 0$  as follows:

In sub-region 1, the electromagnetic eigenmodes can be expressed as

$$E_{z1} = A_{nm} k_{c1}^2 J_n(k_{c1}r) \cos n\theta e^{-\Gamma_{nm}z} \quad (1)$$

$$H_{z1} = B_{nm} k_{c1}^2 J_n(k_{c1}r) \sin n\theta e^{-\Gamma_{nm}z} \quad (2)$$

$$E_{r1} = \left[ -j\omega\mu_1 B_{nm} \frac{n}{r} J_n(k_{c1}r) - A_{nm} \Gamma_{nm} k_{c1} J'_n(k_{c1}r) \right] \cdot \cos n\theta e^{-\Gamma_{nm}z} \quad (3)$$

$$E_{\theta1} = \left[ j\omega\mu_1 B_{nm} k_{c1} J'_n(k_{c1}r) + A_{nm} \Gamma_{nm} \frac{n}{r} J_n(k_{c1}r) \right] \cdot \sin n\theta e^{-\Gamma_{nm}z} \quad (4)$$

$$H_{r1} = \left[ -B_{nm} \Gamma_{nm} k_{c1} J'_n(k_{c1}r) - j\omega\varepsilon_{c1} A_{nm} \frac{n}{r} J_n(k_{c1}r) \right] \cdot \sin n\theta e^{-\Gamma_{nm}z} \quad (5)$$

$$H_{\theta1} = \left[ -B_{nm} \Gamma_{nm} \frac{n}{r} J_n(k_{c1}r) - j\omega\varepsilon_{c1} A_{nm} k_{c1} J'_n(k_{c1}r) \right] \cdot \cos n\theta e^{-\Gamma_{nm}z} \quad (6)$$

In sub-region 2, the electromagnetic eigenmodes can be expressed as

$$E_{z2} = [C_{nm} J_n(k_{c2}r) + D_{nm} Y_n(k_{c2}r)] k_{c2}^2 \cos n\theta e^{-\Gamma_{nm}z} \quad (7)$$

$$H_{z2} = [E_{nm} J_n(k_{c2}r) + F_{nm} Y_n(k_{c2}r)] k_{c2}^2 \sin n\theta e^{-\Gamma_{nm}z} \quad (8)$$

$$E_{r2} = \left\{ -j\omega\mu_2 \frac{n}{r} [E_{nm} J_n(k_{c2}r) + F_{nm} Y_n(k_{c2}r)] - \Gamma_{nm} k_{c2} [C_{nm} J'_n(k_{c2}r) + D_{nm} Y'_n(k_{c2}r)] \right\} \cos n\theta e^{-\Gamma_{nm}z} \quad (9)$$

$$E_{\theta2} = \left\{ j\omega\mu_2 k_{c2} [E_{nm} J'_n(k_{c2}r) + F_{nm} Y'_n(k_{c2}r)] \right.$$

$$+ \Gamma_{nm} \frac{n}{r} [C_{nm} J_n(k_{c2}r) + D_{nm} Y_n(k_{c2}r)] \left. \vphantom{\Gamma_{nm}} \right\} \sin n\theta e^{-\Gamma_{nm}z} \quad (10)$$

$$H_{r2} = \left\{ -\Gamma_{nm} k_{c2} [E_{nm} J'_n(k_{c2}r) + F_{nm} Y'_n(k_{c2}r)] \right. \\ \left. - j\omega \varepsilon_{c2} \frac{n}{r} [C_{nm} J_n(k_{c2}r) + D_{nm} Y_n(k_{c2}r)] \right\} \sin n\theta e^{-\Gamma_{nm}z} \quad (11)$$

$$H_{\theta2} = \left\{ -\Gamma_{nm} \frac{n}{r} [E_{nm} J_n(k_{c2}r) + F_{nm} Y_n(k_{c2}r)] \right. \\ \left. - j\omega \varepsilon_{c2} k_{c2} [C_{nm} J'_n(k_{c2}r) + D_{nm} Y'_n(k_{c2}r)] \right\} \cos n\theta e^{-\Gamma_{nm}z} \quad (12)$$

where

$$k_{c1}^2 = \omega^2 \mu_1 \varepsilon_{c1} + \Gamma_{nm}^2 \quad (13)$$

$$k_{c2}^2 = \omega^2 \mu_2 \varepsilon_{c2} + \Gamma_{nm}^2 \quad (14)$$

and  $\varepsilon_{ci} = \varepsilon_0 \left( \varepsilon_i + \frac{\sigma_i}{j\omega \varepsilon_0} \right)$ ,  $i = 1, 2$ .

Applying the boundary conditions to these Eqs. (1)–(12), we can obtain the characteristic equation for the eigenmodes in region II as

$$\left( \Gamma_{nm} \frac{n}{b} J_n(k_{c1}b) \left( 1 - \frac{k_{c1}^2}{k_{c2}^2} \right) \right)^2 \\ = \omega^2 \{ \mu_2 k_{c2} C_{EFB} [Y'_n(k_{c2}a) J'_n(k_{c2}b) - J'_n(k_{c2}a) Y'_n(k_{c2}b)] \\ + \mu_1 k_{c1} J'_n(k_{c1}b) \} \{ \varepsilon_{c2} k_{c2} C_{CDA} [J_n(k_{c2}a) Y'_n(k_{c2}b) \\ - Y_n(k_{c2}a) J'_n(k_{c2}b)] - \varepsilon_{c1} k_{c1} J'_n(k_{c1}b) \} \quad (15)$$

When  $n = 0$ , the eigenmodes in region II can be either *TM* or *TE* modes. The characteristic equations for the *TM* or *TE* mode are expressed by

$$J_0(k_{c2}a) \left[ \frac{k_{c2} Y_0(k_{c2}b)}{k_{c1} J_0(k_{c1}b)} - \frac{\varepsilon_{c2} Y'_0(k_{c2}b)}{\varepsilon_{c1} J'_0(k_{c1}b)} \right] \\ - Y_0(k_{c2}a) \left[ \frac{k_{c2} J_0(k_{c2}b)}{k_{c1} J_0(k_{c1}b)} - \frac{\varepsilon_{c2} J'_0(k_{c2}b)}{\varepsilon_{c1} J'_0(k_{c1}b)} \right] = 0 \quad (16)$$

$$J'_0(k_{c2}a) \left[ \frac{\mu_2 Y'_0(k_{c2}b)}{\mu_1 J'_0(k_{c1}b)} - \frac{k_{c2} Y_0(k_{c2}b)}{k_{c1} J_0(k_{c1}b)} \right] \\ - Y'_0(k_{c2}a) \left[ \frac{\mu_2 J'_0(k_{c2}b)}{\mu_1 J'_0(k_{c1}b)} - \frac{k_{c2} J_0(k_{c2}b)}{k_{c1} J_0(k_{c1}b)} \right] = 0 \quad (17)$$

Using the relations between  $k_{c1}$ ,  $k_{c2}$  and  $\Gamma_{nm}$  given in Eqs. (13) and (14), we can numerically obtain the propagation constant  $\Gamma_{nm}$  for each eigenmode and then determine the corresponding eigenvalues  $k_{c1}$  and  $k_{c2}$ . Thus, the eigenmodes in this inhomogeneously filled waveguide can be determined.

### 3. ELECTROMAGNETIC FIELDS IN THREE REGIONS

The electromagnetic fields in each region can then be expressed as the infinite summations of the eigenmodes in the corresponding region. Because we assume that there is an excitation probe in region I, the electric field in region I for  $0 \leq z \leq z_1$  can be expressed as

$$\vec{E}_1(\vec{r}) = \int_{V'} \vec{J}(\vec{r}') \cdot \vec{G}(\vec{r}', \vec{r}) dV' \quad (18)$$

where the dyadic Green's function is given by [14]

$$\vec{G}(\vec{r}', \vec{r}) = \sum_{n=1}^{N_1} \frac{-\vec{e}_{n1}(r', \theta')}{2(1 - R_{1n}R_{2n})} (1 + R_{1n}) Z_n \left( \vec{E}_{n1}^+(\vec{r}) + R_{2n} \vec{E}_{n1}^-(\vec{r}) \right) \quad (19)$$

for  $z \geq 0$  and where  $\vec{e}_{n1}(r', \theta')$  is the transverse component of the eigenmode in region I, which is normalized as

$$\int_{CS} \vec{e}_{n1} \cdot \vec{e}_{n1} dS = 1 \quad (20)$$

$\vec{E}_{n1}^{\pm}(\vec{r})$  is the eigenmode propagating in  $\pm z$  direction.  $R_{1n} = -e^{-2\Gamma_n z_0}$  and  $R_n$  are the reflection coefficients of the  $n$ th mode due to the short-circuit termination at  $z = -z_0$  and the discontinuity at  $z = z_1$  in region I, respectively. The wave impedances for the *TE* and *TM* modes are expressed as

$$Z_{nTE} = \frac{j\omega\mu}{\Gamma_n} \quad (21)$$

$$Z_{nTM} = \frac{\Gamma_n}{j\omega\varepsilon} \quad (22)$$

where  $\Gamma_n$  is the wave propagation constant of the  $n$ th mode and is given by  $\Gamma_n^2 = k_{c1}^2 - \omega^2\mu_1\varepsilon_1$  with  $k_{c1}$  as the eigenvalue of the

eigenmode;  $\mu_1$  and  $\varepsilon_1$  are the dielectric parameters of the medium in region I. The upper summation limit  $N_1$  is set to assure a convergent result. The current density on the excitation probe is assumed to have a sinusoidal distribution as

$$\vec{J}(\vec{r}) = \hat{r} I_m \frac{\sin \beta(l - a + r)}{\sin \beta l} \delta(\theta) \delta(z) \quad (23)$$

where  $\beta$  is the wave number in the medium of region I,  $l$  is the length of the excitation probe.

Rewriting the dyadic Green's function (19) as

$$\begin{aligned} \overline{G}(\vec{r}', \vec{r}) = & \sum_{n=1}^{N_1} \frac{-\vec{e}_{n1}(r', \theta')}{2} (1 + R_{1n}) Z_n \vec{E}_{n1}^+(\vec{r}) + \sum_{n=1}^N \frac{-\vec{e}_{n1}(r', \theta')}{2(1 - R_{1n}R_{2n})} \\ & \cdot (1 + R_{1n}) R_{2n} Z_n \left[ R_{1n} \vec{E}_{n1}^+(\vec{r}) + \vec{E}_{n1}^-(\vec{r}) \right] \end{aligned} \quad (24)$$

and substituting Eq. (24) into Eq. (18), we can obtain the electric field in region I as:

$$\vec{E}_1(\vec{r}) = \sum_{n=1}^{N_1} V_n e^{\Gamma_n z_1} \vec{E}_{n1}^+(\vec{r}) + \sum_{n=1}^{N_1} A_n e^{-\Gamma_n z_1} \left[ R_{1n} \vec{E}_{n1}^+(\vec{r}) + \vec{E}_{n1}^-(\vec{r}) \right] \quad (25)$$

where

$$V_n = -\frac{1 + R_{1n}}{2} Z_n e^{-\Gamma_n z_1} \int \left[ \vec{e}_{n1}(r', \theta') \cdot \vec{J}(\vec{r}') \right] dV' \quad (26)$$

is known and

$$A_n = -\frac{1 + R_{1n}}{2(1 - R_{1n}R_{2n})} R_{2n} Z_n e^{\Gamma_n z_1} \int \left[ \vec{e}_{n1}(r', \theta') \cdot \vec{J}(\vec{r}') \right] dV' \quad (27)$$

is unknown due to the unknown reflection coefficient  $R_{2n}$ . The magnetic field in region I can also be expressed as

$$\vec{H}_1(\vec{r}) = \sum_{n=1}^{N_1} V_n e^{\Gamma_n z_1} \vec{H}_{n1}^+(\vec{r}) + \sum_{n=1}^{N_1} A_n e^{-\Gamma_n z_1} \left[ R_{1n} \vec{H}_{n1}^+(\vec{r}) + \vec{H}_{n1}^-(\vec{r}) \right] \quad (28)$$

where  $\vec{H}_{n1}^{\pm}(\vec{r})$  is the eigenmode propagating in  $\pm z$  direction.

In region II,  $z_1 \leq z \leq z_2$ , the electromagnetic fields can be represented as

$$\vec{E}_2(\vec{r}) = \sum_{m=1}^M \left[ B_m e^{\Gamma_m z_1} \vec{E}_{m2}^+(\vec{r}) + C_m e^{-\Gamma_m z_2} \vec{E}_{m2}^-(\vec{r}) \right] \quad (29)$$

$$\vec{H}_2(\vec{r}) = \sum_{m=1}^M \left[ B_m e^{\Gamma_m z_1} \vec{H}_{m2}^+(\vec{r}) + C_m e^{-\Gamma_m z_2} \vec{H}_{m2}^-(\vec{r}) \right] \quad (30)$$

where  $\vec{E}_{m2}^{\pm}(\vec{r})$  and  $\vec{H}_{m2}^{\pm}(\vec{r})$  denote the electromagnetic eigenmodes propagating in  $\pm z$  direction.

In region III,  $z_2 \leq z \leq z_3$ , the electromagnetic fields can be represented as

$$\vec{E}_3(\vec{r}) = \sum_{n=1}^{N_2} D_n e^{\Gamma_n z_2} \left[ \vec{E}_{n1}^+(\vec{r}) + R_n \vec{E}_{n1}^-(\vec{r}) \right] \quad (31)$$

$$\vec{H}_3(\vec{r}) = \sum_{n=1}^{N_2} D_n e^{\Gamma_n z_2} \left[ \vec{H}_{n1}^+(\vec{r}) + R_n \vec{H}_{n1}^-(\vec{r}) \right] \quad (32)$$

where  $R_n = -e^{-2\Gamma_n c}$  is the reflection coefficient at the termination of  $z = z_3$ .

Applying the boundary conditions at the junctions of each region, we obtain the equations for the unknown coefficients  $B_m$  and  $C_m$  as

$$[BM_1]_{N_1 \times M} [B]_{M \times 1} + [CM_1]_{N_1 \times M} [C]_{M \times 1} = [VS]_{N_1 \times 1} \quad (33)$$

$$[BM_2]_{N_2 \times M} [B]_{M \times 1} + [CM_2]_{N_2 \times M} [C]_{M \times 1} = [0]_{N_2 \times 1} \quad (34)$$

where the elements in each matrix are expressed as

$$BM_{1nm} = \frac{e_{mn}}{1 - e^{-2\Gamma_n(z_1+z_0)}} + \frac{Z_n^2 h_{mn}}{1 + e^{-2\Gamma_n(z_1+z_0)}} \quad (35)$$

$$CM_{1nm} = \frac{e^{\Gamma_m(z_1-z_2)} e_{mn}}{1 - e^{-2\Gamma_n(z_1+z_0)}} - \frac{Z_n^2 e^{\Gamma_m(z_1-z_2)} h_{mn}}{1 + e^{-2\Gamma_n(z_1+z_0)}} \quad (36)$$

$$e_{mn} = \int_{CS} \vec{e}_{n1} \cdot \vec{e}_{m2} dS \quad (37)$$

$$h_{mn} = \int_{CS} \vec{h}_{n1} \cdot \vec{h}_{m2} dS \quad (38)$$

$$VS_n = \frac{2V_n}{1 - e^{-4\Gamma_n(z_1+z_0)}} \quad (39)$$

$$[B]_{M \times 1} = [B_1, B_2, \dots, B_M]^T \quad (40)$$

$$[C]_{M \times 1} = [C_1, C_2, \dots, C_M]^T \quad (41)$$

If we choose  $N_1 = N_2 = M$ , the matrices  $[BM_1]$ ,  $[CM_1]$ ,  $[BM_2]$ , and  $[CM_2]$  in Eqs. (33) and (34) are square matrices and the solutions for  $B_m$  and  $C_m$  can be expressed as

$$[B]_{M \times 1} = [[BM_1] - [CM_1][CM_2]^{-1}[BM_2]]^{-1} [VS] \quad (42)$$

$$[C]_{M \times 1} = [[CM_1] - [BM_1][BM_2]^{-1}[CM_2]]^{-1} [VS] \quad (43)$$

After the unknown coefficients  $B_m$  and  $C_m$  are obtained from Eqs. (42) and (43), we may determine the electromagnetic fields in region II; that is, the induced electric field in the material sample can be quantified. The unknown coefficients  $A_n$ ,  $D_n$  and the electromagnetic fields in regions I and III can be obtained based on the numerical results of region II.

#### 4. NUMERICAL EXAMPLES

In this section, the numerical results based on the mode-matching method will be demonstrated. As stated before, we restrict the material samples which are placed in a cylindrical waveguide to be of simple cylindrical shapes and homogeneous. The numerical results obtained will be compared with the corresponding results derived using the integral equation method [1].

In the numerical computation, the eigenmodes in region II are derived first after the dimensions and the dielectric parameters of the material sample are selected. The integrations of product of the eigenmodes in regions I and II (given in Eqs. (37) and (38)) are then calculated. After the total electromagnetic fields are obtained, their numerical results can be checked further by the boundary conditions at the perfectly conducting walls and at the junctions of the different regions.

Examining the matrix Eqs. (33) and (34), we find that when  $VS_n = 0$  for some indices  $n$ , the solutions for  $B_m$  and  $C_m$  become zero also. Thus, we can select the eigenmodes based on both the values of  $VS_n$  and the convergence property of the summation for the electromagnetic fields in each region.

In the following numerical computations, we assume the dimensions of the cylindrical waveguide shown in Fig. 1 to be: the radius  $a = 0.0762$  m and the length  $c = 0.15458$  m. A cylindrical material sample with the dimensions of radius  $r_0$  and length  $h_0$  is placed in the center of the waveguide. The position of the excitation probe is at  $c/4$  from the bottom of the waveguide, that is,  $z_0 = \frac{c}{4}$  and  $z_3 = \frac{3 \times c}{4}$ . The values of  $b$ ,  $z_1$  and  $z_2$  are determined by the dimensions of the material sample to be  $b = r_0$ ,  $z_1 = \frac{c}{2} - \frac{h_0}{2} - z_0$ , and  $z_2 = \frac{c}{2} + \frac{h_0}{2} - z_0$ . The length of the excitation probe is chosen as the half of the radius of the waveguide,  $a/2$ , and the operating frequency is 2.45 GHz. The relative permittivity of the material sample is assumed to be  $\epsilon_r = 2.5$  and it is lossless.

Several special cases with selected shapes and dimensions of the material sample, which can be compared with some theoretical approximations, have been studied.

#### 4.1 Cubic-Like Material Sample

A cubic-like material sample, having the diameter equal to the length, is placed in the center of the cylindrical waveguide. The dimensions of the material sample are chosen as: radius  $r_0 = 0.004$  m and length  $h_0 = 0.008$  m.

In the numerical computation, the number of modes to be summed is set to be 62 based on the non-zero values of the right hand side of the Eq. (33). However, observing the numerical results for the solutions of the unknown coefficients  $A_n$  and  $D_n$  in regions I and III, we find that there only exist several waveguide modes with significant magnitudes which are shown in Table 1; the  $TM_{01}$  mode appears as the dominant mode. This result is expected because of the choice of the dimensions of the cylindrical waveguide and the operating frequency of the excitation probe. The computational results show that the electromagnetic fields in each region do not vary significantly with respect to the variable  $\theta$  and the  $z$  component of the induced electric field dominates the other two components of the electric field near the center of the waveguide.

Fig. 3 demonstrates the ratio of the  $z$  component of the induced electric field in the material sample to that of the electric field near the material sample in the empty region of the waveguide as a function of  $z$  at  $r = 0.0004$  m. The ratios are around 0.69 to 0.72 which are close to 0.667 given by the electrostatic estimation of  $E_z/E_z^i = \frac{3}{2+\epsilon_r}$ .

For a larger cubic-like material sample with the dimensions:  $r_0 =$

**Table 1.** Significant modes in the mode-matching method when the dimensions of the cavity are:  $a = 0.0762$  m,  $c = 0.15458$  m and that of the material sample are:  $r_0 = 0.004$  m and  $h_0 = 0.008$  m. The operating frequency is 2.45 GHz, and the excitation probe is located at  $c/4$  from the bottom.

| Mode      | $A_n$ (real, imaginary) | $D_n$ (real, imaginary) |
|-----------|-------------------------|-------------------------|
| $TM_{01}$ | -79.1583, 11.9465       | 78.8164, -14.0405       |
| $TM_{02}$ | 0, 0.5485               | 0, 0.3906               |
| $TM_{03}$ | 0, 0.8847               | 0, -0.8946              |
| $TM_{04}$ | 0, -1.1825              | 0, 1.1827               |
| $TM_{05}$ | 0, 1.4291               | 0, -1.4276              |
| $TM_{06}$ | 0, -1.6162              | 0, 1.6144               |
| $TM_{07}$ | 0, 1.7506               | 0, -1.7483              |
| $TM_{11}$ | -0.1651, 0.1809         | 0.1798, 0.1671          |
| $TM_{12}$ | -3.8618, 2.3057         | 4.4303, 0.7882          |

0.01 m and  $h_0 = 0.02$  m, the number of the modes is set to be 76. The most significant values for the unknown coefficients  $A_n$  and  $D_n$  in regions I and III still belong to the  $TM_{01}$  waveguide mode. Therefore, the  $z$  component of the induced electric field dominates near the center of the waveguide. Fig. 4 shows the ratio of the  $z$  component of the induced electric field in the material sample to that of the electric field in the empty waveguide near the material sample varying as a function of  $r$  at the different locations of  $z$ . Due to the symmetric property of the numerical solutions, we only plot the ratios in the lower half of the material sample in Fig. 4. The corresponding results generated from an integral equation method [1] are plotted in the same figure for comparison. We observe a good agreement between these two sets of numerical results generated by two different methods.

## 4.2 Thin Disk Material Sample

A material sample with the shape of a thin disk, having its length much smaller than its diameter, is placed in the center of the cylindrical waveguide. The dimensions of the material sample are  $h_0 = 0.001$  m and  $r_0 = 0.02$  m and the number of the modes which are involved in the computation is 55. The numerical results are shown in Fig. 5.

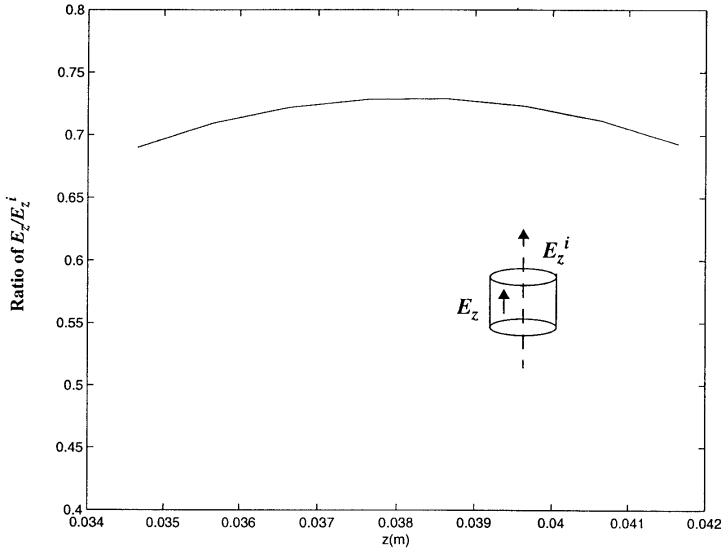


**Figure 3.** Ratio of  $E_z/E_z^i$  varies in the  $z$  direction at  $r = 0.0004$  m. The dimensions of the material sample are  $r_0 = 0.004$  m and  $h_0 = 0.008$  m with the relative permittivity of  $\epsilon_r = 2.5$ . The dimensions of the cylindrical waveguide are:  $a = 0.0762$  m and  $c = 0.15458$  m. The operating frequency is 2.45 GHz.

Since the  $z$  component of the induced electric field dominates near the center of the waveguide, the ratios of the  $z$  component of the induced electric field to that of the electric field near the material sample in the empty region of the waveguide are plotted as a function of the radial distance,  $r$ , in Fig. 5. We observe that the numerical results are close to the theoretical estimation given by the boundary condition of  $E = (1/\epsilon_r)E^i = 0.4E^i$ .

### 4.3 Thin Dielectric Rod Material Sample

A material sample with the dimensions: the length  $h_0 = 0.044$  m and the radius  $r_0 = 0.004$  m, is placed in the center of the cylindrical waveguide. The number of the modes involved in the computation is 129 and the numerical result is shown in Fig. 6.

Examining the numerical results for the solutions of the unknown coefficients  $A_n$  and  $D_n$  in regions I and III, we find that those with the most significant values belong to the  $TM_{01}$  waveguide mode; that

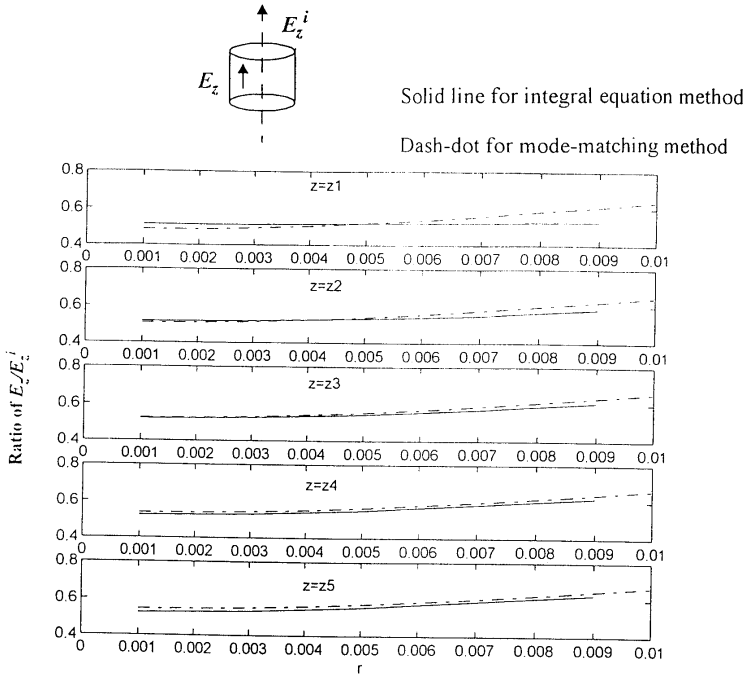


**Figure 4.** Ratio of  $E_z/E_z^i$  varies in the  $r$  direction at the different locations of  $z$ , obtained from the mode-matching method and the integral equation method [1]. The dimensions of the material sample are  $r_0 = 0.01$  m and  $h_0 = 0.02$  m with the relative permittivity of  $\epsilon_r = 2.5$ . The dimensions of the cylindrical waveguide are:  $a = 0.0762$  m and  $c = 0.15458$  m. The operating frequency is 2.45 GHz.

is, the  $TM_{01}$  waveguide mode dominates in the empty region of the waveguide. For this case, the induced electric field inside the material sample should be approximately equal to the electric field in the empty region near the material sample for the following reasons: First, the electric field in the empty region near the material sample or near the center of the waveguide is dominated by the  $z$  component and it is tangential to the major part of the material sample surface. Secondly, the continuity of the tangential component of the electric field at the material sample surface requires this estimation.

In Fig. 6, we plot the ratios of the  $z$  component of the induced electric field to that of the electric field near the material sample in

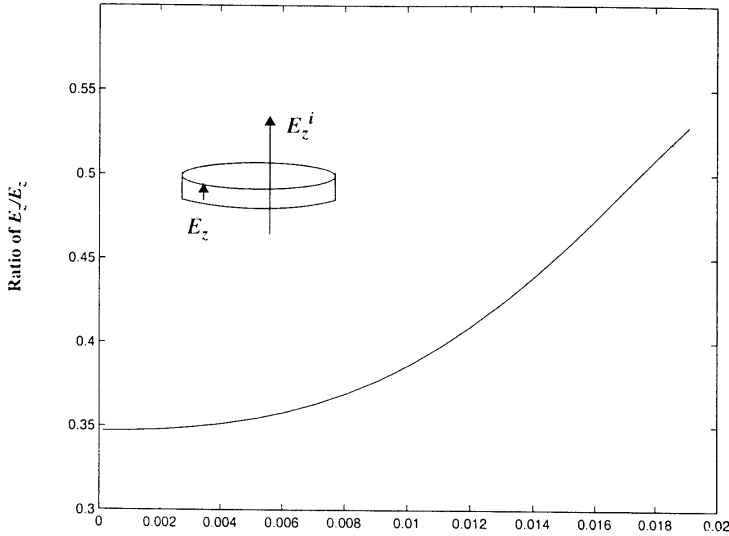


**Figure 5.** Ratio of  $E_z/E_z^i$  varies in the  $r$  direction. The dimensions of the material sample are  $r_0 = 0.02$  m and  $h_0 = 0.001$  m with the relative permittivity of  $\varepsilon_r = 2.5$ . The dimensions of the cylindrical waveguide are:  $a = 0.0762$  m and  $c = 0.15458$  m. The operating frequency is 2.45 GHz.

the empty region of the waveguide varying as a function of  $z$  at  $r = 0.0004$  m. Most of the ratios are very close to 1 which is in agreement with the theoretical estimation.

Considering the numerical accuracy and the computation time, we find that in the mode-matching method the number of the modes to be summed can be reduced a great deal when compared with the integral equation method. The most important reason for this finding is that the eigenmodes used in the mode-matching method satisfy the boundary conditions on the material sample and the cavity wall. (On the other hand, the vector wave functions used in the integral equation method only satisfy the boundary conditions at the cavity wall.)

The other reason for this finding is that in the mode-matching method, the angular dependence of the eigenmodes,  $\vec{e}_{n1}$ ,  $\vec{e}_{m2}$ ,  $\vec{h}_{n1}$ , and  $\vec{h}_{m2}$ , on  $\theta$  is  $\sin n\theta$  or  $\cos n\theta$ , and many of the integrations of the scalar products of these eigenmodes given in Eqs. (37) and (38) become zero due to the orthogonality of the sinusoidal functions. Therefore, the matrices  $[BM_1]$ ,  $[CM_1]$ ,  $[BM_2]$ , and  $[CM_2]$  given in Eqs. (33)

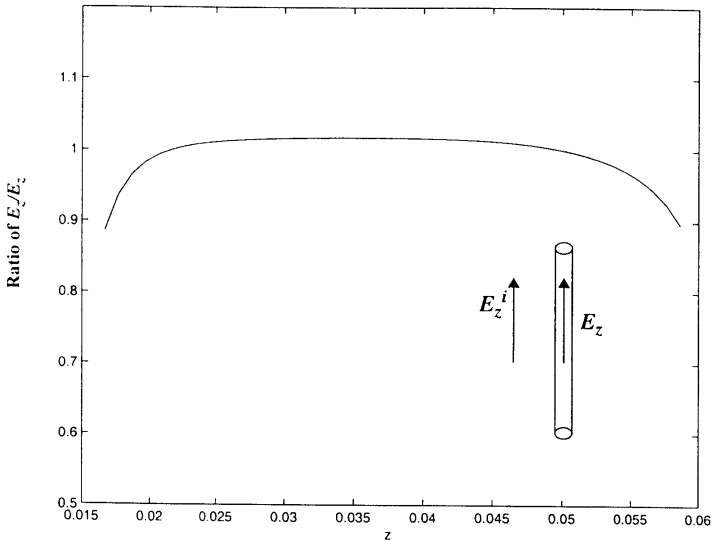


**Figure 6.** Ratio of  $E_z/E_z^i$  varies in the  $z$  direction at  $r = 0.0004$  m. The dimensions of the material sample are  $r_0 = 0.004$  m and  $h_0 = 0.044$  m with the relative permittivity of  $\epsilon_r = 2.5$ . The dimensions of the cylindrical waveguide are:  $a = 0.0762$  m and  $c = 0.15458$  m. The operating frequency is 2.45 GHz.

and (34) are sparse and the computation time can be saved greatly. In spite of this advantage for the mode-matching method, it is not a very general technique because it can not be used to solve the problem involving material samples with arbitrary shapes or heterogeneous compositions.

## 5. CONCLUSIONS

In this paper, the mode-matching method is applied to the case of the homogeneous material sample with a simple geometry and it is found that the mode-matching method can save a great deal of computation time when compared with the integral equation method. This can be attributed to the use of the well-defined eigenmodes and sparse resultant matrices. Numerical results obtained agree well with that of the integral equation method.

## ACKNOWLEDGMENT

This paper was supported by the National Science Foundation under Grant No. CTS 9526038 and The State of Michigan under a Research Excellence Fund.

## REFERENCES

1. Zhang, J., and K. M. Chen, "Quantification of the induced electric field in a material sample placed within an energized cylindrical cavity," current issue.
2. Zaki, K. A., and A. E. Atia, "Modes in dielectric-loaded waveguides and resonators," *IEEE Trans. on Microwave Theory and Technologies*, Vol. MTT-31, No. 12, 1039–1045, Dec. 1983.
3. Kajbez, D., A. V. Glisson, and J. James, "Computed modal field distribution for isolated dielectric resonators," *1984 IEEE MTT-S International Microwave Symposium Digest*, 193–195, June 1984.
4. Zaki, K. A., and C. Chen, "Intensity and distribution of hybrid-mode fields in dielectric-loaded waveguides," *IEEE Trans. on Microwave Theory and Technologies*, Vol. MTT-33, No. 12, 1442–1447, Dec. 1985.
5. Maj, S., and M. Pospieszalski, "A composite cylindrical dielectric resonator," *1984 IEEE MTT-S International Microwave Symposium Digest*, 190–192, June 1984.
6. Krupka, J., "Optimization of an electromagnetic basis for determination of the resonant frequency of microwave cavities partially filled with a dielectric," *IEEE Trans. on Microwave Theory and Technologies*, Vol. MTT-31, No. 3, 302–305, March 1983.
7. Kajfez, D., A. V. Glisson, and J. James, "Computed modal field distribution for isolated dielectric resonators," *IEEE Trans. on Microwave Theory and Technologies*, Vol. MTT-32, No. 12, 1609–1616, Dec. 1984.
8. Ayappa, K. G., H. T. Davis, E. A. Davis, and J. Gordon, "Two-dimensional finite element analysis of microwave heating," *AICHE Journal*, Vol. 38, 1577–1592, Oct. 1992.
9. Jia, X., and P. Jolly, "Simulation of microwave field and power distribution in a cavity by a three-dimensional finite element method," *Journal of Microwave Power and Electromagnetic Energy*, Vol. 27, No. 1, 11–22, 1992.

10. Liu, F., I. Turner, and M. Bialkowski, "A finite-difference time-domain simulation of power density distribution in a dielectric loaded microwave cavity," *Journal of Microwave Power and Electromagnetic Energy*, Vol. 29, 138–148, 1994.
11. Zhao, H., I. Turner, and F. W. Liu, "Numerical simulation of the power density distribution generated in a multimode cavity by using the method of lines technique to solve directly for the electric field," *IEEE Trans. on Microwave Theory and Technologies*, Vol. MTT-44, 2185–2194, 1996.
12. Torres, F., and B. Jecko, "Complete FDTD analysis of microwave heating processing in frequency-dependent and temperature-dependent media," *IEEE Trans. Microwave Theory Tech.*, Vol. MTT-45, 108–117, 1997.
13. Fu, W., and A. Metaxas, "Numerical prediction of three-dimensional power density distribution in a multi-mode cavity," *Journal of Microwave Power and Electromagnetic Energy*, Vol. 29, 67–75, 1994.
14. Collin, R. E., *Field Theory of Guided Waves*, second edition, IEEE Press, 1991.